Spectrochimica Acta Part A: Molecular and Biomolecular Spectroscopy 114 (2013) 129–136

Contents lists available at SciVerse ScienceDirect

Spectrochimica Acta Part A: Molecular and Biomolecular Spectroscopy

journal homepage: www.elsevier.com/locate/saa

FT-IR, dispersive Raman, NMR, DFT and antimicrobial activity studies on 2-(Thiophen-2-yl)-1*H*-benzo[*d*]imidazole

Arslan Ünal [a,*], Bilge Eren [b]

[a] Department of Physics, Bilecik Şeyh Edebali University, 11210 Bilecik, Turkey
[b] Department of Chemistry, Bilecik Şeyh Edebali University, 11210 Bilecik, Turkey

HIGHLIGHTS

- 2-(Thiophen-2-yl)-1*H*-benzo[*d*] imidazole was synthesized under microwave conditions.
- It was characterized by FT-IR, dispersive-Raman, NMR and DFT.
- Conformational stability was examined.
- A detailed interpretations of the vibrational modes were reported.
- The antimicrobial activities of title compound were also tested.

GRAPHICAL ABSTRACT

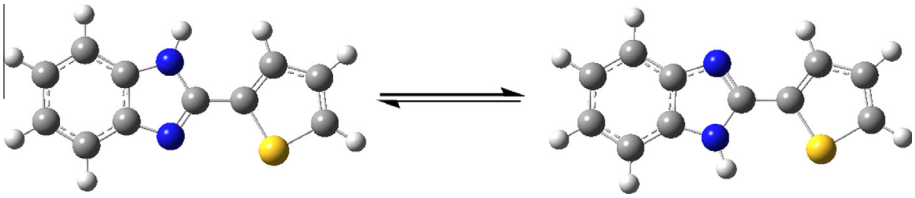

ARTICLE INFO

Article history:
Received 18 January 2013
Received in revised form 13 May 2013
Accepted 14 May 2013
Available online 29 May 2013

Keywords:
Benzimidazole
Thiophene
2-(Thiophen-2-yl)-1*H*-benzo[*d*]imidazole
Vibrational spectra
NMR
DFT

ABSTRACT

2-(Thiophen-2-yl)-1*H*-benzo[*d*]imidazole (TBI) was synthesized under microwave conditions and was characterized by FT-IR, dispersive Raman, ^{1}H-, ^{13}C-, DEPT-, HETCOR-NMR spectroscopies and density functional theory (DFT) computations. The FT-IR and dispersive Raman spectra of TBI were recorded in the regions 4000–400 cm^{-1} and 4000–100 cm^{-1}. The experimental vibrational spectra were interpreted with the help of normal coordinate analysis based on DFT/B3LYP/6-311++G(d,p) theory level for the more stable tautomeric form (Tautomer 1). The complete vibrational assignments were performed on the basis of the potential energy distribution (PED) of the vibrational modes, calculated with scaled quantum mechanical (SQM) method. A satisfactory consistency between the experimental and theoretical findings was obtained. The frontier molecular orbitals (FMOs), atomic charges and NMR shifts of the two stable tautomeric forms were also obtained at the same theory level without any symmetry restrictions. In addition, the title compound was screened for its antimicrobial activity and was found to be exhibit antifungal and antibacterial effects.

Introduction

It is well known that benzimidazole derivatives possess a variety of biological activities. They shows broad spectrum of pharmacological effects. Several compounds containing benzimidazole group have been reported to exhibit antimicrobial [1–3], anticancer [4,5] antifungal [6,7], antiparasitic [8], antiviral [9] and anti-inflammatory [10] activities. Particularly, thiophene benzimidazole compounds are novel, selective and potent inhibitors of polo-like kinase 1 (PLK1) that play critical roles in regulating processes in cell cycle. They inhibit the proliferation of a wide variety of tumor cell lines of diverse origin [11,12]. In the view of these facts, benzimidazole compounds have attracted many scientists to investigate the structural and spectral behaviors of them that necessary for understanding their chemical or biological properties [13–15].

The combination of vibrational (IR, Raman) and NMR spectroscopy coupled with quantum mechanical calculations are extensively used for understanding the dynamical and structural properties of organic or inorganic molecules. With the recent developments in computational methods, it is possible to describe chemical and physical properties of molecules with close accuracy using theoretical methods [16,17]. The density functional theory

* Corresponding author. Tel.: +90 228 214 1479; fax: +90 228 216 0080.
E-mail address: arslan.unal@bilecik.edu.tr (A. Ünal).

1386-1425/$ - see front matter © 2013 Elsevier B.V. All rights reserved.
http://dx.doi.org/10.1016/j.saa.2013.05.045

(DFT) calculations using hybrid B3LYP method exhibits excellent performance on electrostatic potentials, optical properties, vibrational wavenumbers, NMR shifts and geometric structures of organic compounds [18–26].

To the best of our knowledge, neither quantum chemical calculations nor the vibrational spectra of 2-(Thiophen-2-yl)-1*H*-benzo[*d*]imidazole (TBI) have been reported in the open scientific literature to date. Therefore, TBI was initially synthesized under neat microwave conditions, was secondly characterized by FT-IR, dispersive-Raman, ^{13}C-, ^{1}H-, DEPT-, HETCOR-NMR spectroscopies and was finally screened for its antimicrobial activity. The local minimum and transition state forms of TBI on its potential energy surface (PES) were defined by using DFT/B3LYP/6-311++G(d,p) theory level. A complete assignment of the vibrational modes was also performed for the more stable tautomeric form (Tautomer 1 = T1) with the aid of the potential energy distribution (PED) values by using the scaled quantum mechanical (SQM) method. In addition, frontier molecular orbitals (FMOs), natural bond orbitals (NBOs) and NMR spectroscopic features were analyzed for two stable tautomers (T1 and T2) at the same theory level without any symmetry restrictions. These calculations are also valuable for providing insight into molecular parameters, vibrational and NMR spectra. The aim of this work is to explore the structural parameters, spectroscopic and biological features of the title compound that rules its chemical behavior.

Experimental details

Instrumentation

All the chemicals and solvents were of analytical grade and used without any further purification. Reactions under microwave irradiation were performed in a modified domestic microwave oven (Bosch HMT 812C). Reactions were monitored by thin-layer chromatography (TLC) on silica-gel 60 F254 plates (Merck) and an UV lamp. The melting point was determined using a capillary tube and a digital melting point apparatus (Gallenkamp Electrothermal) and was uncorrected. The ATR-IR spectrum of TBI was recorded in the range of 4000–500 cm^{-1} with a Bruker Vertex 80v FTIR spectrometer. The FT-IR (4000–400 cm^{-1}) spectra between KBr windows as Nujol or 1,3-hexachlorobutadiene mulls of the sample were recorded via a Bruker Optics IFS66v/s FTIR spectrometer with 2 cm^{-1} resolution in vacuum. The dispersive Raman spectrum was recorded using a Bruker Senterra Dispersive Raman microscope spectrometer at 532 nm excitation from a doubled Nd/YAG laser having 3 cm^{-1} resolution between 3700 and 60 cm^{-1} spectral region. ^{1}H-, ^{13}C-, DEPT135 and HETCOR-NMR spectra were analyzed on a Bruker Ultra Shield Plus-400 MHz NMR spectrometer using TMS as an internal standard and DMSO-d_6 as solvent.

Synthesis of 2-(Thiophen-2-yl)-1H-benzo[d]imidazole

2-(Thiophen-2-yl)-1*H*-benzo[*d*]imidazole was obtained by condensation of o-phenylenediamine with the $NaHSO_3$ adduct of 2-thiophenecarboxaldehyde according to Ridley et al. [27], but under neat microwave conditions. 2-Thiophenecarboxaldehyde 4.57 g (40 mmol) was dissolved in 20 ml ethanol and $NaHSO_3$ 4.16 g (40 mmol) in 20 ml water was added in portions. The mixture was stirred vigorously an hour in an ice bath. The precipitate was $NaHSO_3$ adduct of 2-thiophenecarboxaldehyde, filtered as white solid and dried under vacuo 4.4 g (yield: 50%). 2 mmol (0.22 g) o-phenylenediamine and 2 mmol (0.432 g) $NaHSO_3$ adduct of 2-thiophenecarboxaldehyde were mixed. After adding a few drops of dimethylformamide, the mixture was irradiated in a modified domestic microwave oven for 6 min until the reaction was completed according to the TLC data. The mixture was cooled and poured onto ice cold water under vigorous stirring. The precipitate was collected by filtration, washed with water and crystallized from ethanol/water. Colorless needle crystals were obtained: 0.3 g, yield 75%, m.p. 333–334 °C (m.p. 332–334 °C is also reported in Ref. [28]). The synthesis procedure of 2-(Thiophen-2-yl)-1*H*-benzo[*d*]imidazole is shown in Scheme 1.

Bacterial strains and assays for in vitro antibacterial activity

Antimicrobial activities were determined by using culture of *Bacillus subtilis* NRRL B-209, *Staphylococcus aureus* ATCC 25923 as Gram positive bacteria and *Escherichia coli* ATCC 25922, *Pseudomonas aeruginosa* ATCC 27853 as Gram negative bacteria and *Saccharomyces cerevisiae* ATCC 9763 as yeast and *Aspergillus parasiticus* NRRL 1957, *Candida albicans* ATCC 10231 as fungus.

The minimal inhibitory concentrations (MICs) of TBI, against tested bacteria were determined by using a broth microdilution method in 96 multi-well microtitre plates [29]. After overnight cultivation, bacterial suspensions were made in Mueller Hinton broth and their turbidity was standardized to 0.5 McFarland. Dimethyl sulphoxide was used to dissolve and to dilute sample. A serial double dilution of the sample was prepared in 96 well microtitre plates, using method of Sarker et al. [30]. The stock concentration was 20 mg/ml. The lowest concentration of the sample that inhibited visible growth was taken as the MIC value. To determine minimal bactericidal concentration (MBC), broth was taken from each well without visible growth and inoculated in Mueller Hinton agar for 24 h at 37 °C. The lowest concentration of the tested sample that killed 99.9% of bacterial cells was evaluated as the MBC value. Tests were carried out in triplicate.

Computational details

A preliminary search of low-energy structures was performed by using Becke's three-parameter exchange functional [18] in combination with the Lee–Yang–Parr correlation functional [31] (B3LYP) method with split-valence polarized 6-311++G(d,p) basis set as implemented in Gaussian03W program package [32]. Conformational energies were calculated as a one-dimensional scan by varying the N2—C7—C8—S1 torsion angle from 0° to 360° in steps of 1°, and the potential energy surface (PES) map was obtained. The optimum four geometric structures concerning to local minima or transition states on the PESs were then examined through optimization and vibrational frequency analysis at the same level of theory. At the optimized structure of examined species, no imaginary wavenumber modes were obtained, providing that a true minimum on the PESs was found. The computations showed that TBI have two stable tautomers with imposing C_1 point group. However, the other appropriate point group such as C_s was taken into account before calculating spectroscopic features of the tautomeric forms. The rotational potential barrier for the selected torsion angle was defined as the energy difference between the highest energy conformation and the energy of the equilibrium structure. The Gibbs free energy values (ΔG), which were calculated at B3LYP/6-311++G(d,p) within the harmonic approximation, were used for the evaluation of the tautomeric mole fractions [33].

The potential energy distribution (PED) calculations which show the relative contributions of the redundant internal coordinates to each normal vibrational mode of the molecule and thus make it possible to describe the character of each mode numerically were carried out by scaled quantum mechanic (SQM) method [34,35]. The relative Raman intensity (I^R), which simulates the measured Raman spectrum, was calculated by using the following

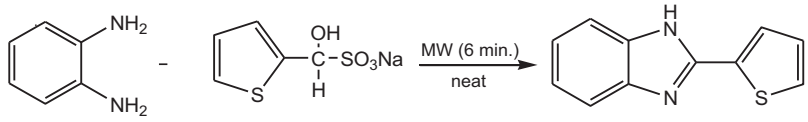

Scheme 1. Synthesis of 2-(Thiophen-2-yl)-1*H*-benzo[*d*]imidazole.

relation derived from the intensity theory of Raman scattering [21];

$$I_i^R = \frac{f(v_0 - v_i)^4 S_i}{v_i[1 - \exp(-hcv_i/kT)]} \quad (1)$$

where v_0 is the exciting wavenumber (18,798 cm^{-1}), v_i is the vibrational wavenumber of the *i*th normal mode (in cm^{-1} units), S_i is the Raman scattering activity of the normal mode q_i, h, c, k are fundamental constants, T = 298.15 K and f is a suitably chosen common normalization factor for all peaks. For the plots of simulated IR and Raman spectra, pure Lorentzian band shapes were used with a bandwidth of 10 cm^{-1}.

Main atomic charges of non-hydrogen atoms using the natural population analysis (NPA) analysis and frontier molecular orbitals (FMOs) were obtained at the same level of theory. For the NMR calculations, the tautomers of TBI molecule were initially optimized at B3LYP/6-311++G(d,p) theory level in DMSO-d_6 by using the integral equation formalism polarizable continuum model (IEFPCM) method [36,37]. After optimization, ^{1}H and ^{13}C NMR isotropic shielding tensors of the title compound were calculated gauge including atomic orbital (GIAO) method [38,39] in DMSO-d_6 at the same theory level as implemented in Gaussian 03W program package. Isotropic shielding tensors of ^{13}C and ^{1}H were changed into chemical shifts by using a linear relationship suggested by Alyar et al. [24].

Results and discussion

Geometrical structures

To define the preferential position of the benzimidazole ring system with respect to the thiophene ring, a preliminary search of low-energy structures was performed by using DFT computation without any symmetry restrictions as a function of the selected torsion angle, τ(N2—C7—C8—S1). The calculated one dimensional PES of TBI with respect to rotations about the selected torsion angle is presented in Fig. S1 (Supplementary material). According to the PES results, two low-energy structures for τ(N2—C7—C8—S1) are located at 0° and 180° with energies of −584744.017 and −584743.576 kcal/mol, respectively. As expected two high-energy structures corresponding to the transition states for τ(N2—C7—C8—S1) are located at 90° and 270° have the same energy which was −584739.434 kcal/mol. The total electronic energy difference between the most favorable and most unfavorable conformers, which arises from the rotational potential barrier calculated with respect to the selected torsion angle, is calculated to be 4.441 kcal/mol.

The results of the DFT computations have clearly demonstrated that TBI has two stable tautomers at room-temperature which are shown in Fig. 1. The calculated relative energies of Tautomer 1 (T1) and Tautomer 2 (T2) are presented in Table 1. The total electronic energy (E_{total}) and zero point corrected total energy (E_0) of each tautomers are quite similar, with no more than a 0.5 kcal/mol difference between the tautomers at the B3LYP/6-311G++(d,p) level of theory. The relative stability of each tautomer was also investigated by tautomeric mole fraction according to their Gibbs free energy (ΔG) and thermal energy corrected Gibbs free energy (ΔG^*). The tautomeric mole fraction calculations show that the stability order for the tautomeric forms is T1 > T2 in any symmetry group. On account of energy and tautomeric equilibrium analyses, the T1 form in C_s symmetry group was only considered in the vibrational spectral analysis of TBI.

The optimized skeletal geometric parameters (bond lengths and bond angles) obtained at B3LYP/6-311++G(d,p) for TBI are presented in Table 2 in accordance with atom numbering given in Fig. 1. The weaknesses of X-ray scattering intensities for the obtained needle crystals are not enough to determine the experimental geometric parameters of TBI. Therefore, our optimized structural parameters were compared with the XRD data of closely related molecule 2-(Thiophen-2-yl)-1-(Thiophen-2-ylmeth-yl)-1*H*-benzimidiazaole [40] as given in Table 2.

TBI molecule is composed of a 1*H*-benzo[*d*]imidazole and a thiophene ring. Interestingly, the thiophene and the 1*H*-benzo [*d*]imidazole rings of the molecule are co-planar. The dihedral angles N1—C7—C8—S1 and N1—C7—C8—C9 are 180° and 0°, respectively. Since, there is a full conjugation between p orbitals of all atoms over the molecule.

The imine (C=N) bond length is expected to be shorter than the amine (C—N) bond length. In the T1 of TBI molecule, the imine C7=N2 and amine C7—N1 bond distances are 1.315 and 1.384 Å, respectively. The essential skeletal angles of C1—N1—C7, C2—N2—C7 and C8—S1—C11 are also 107.19°, 105.67° and 91.30°, respectively. These values are particularly in excellent agreement with the values of 2-(Thiophen-2-yl)-1-(Thiophen-2-ylmeth-yl)-1*H*-benzimidiazaole [1.316, 1.376 Å and 106.23°, 105.12°, 91.82°] [40] and1-(thiophene-2-yl-methyl)-2-(thiophene-2-yl)-1*H*-benzimidiazole [1.315, 1.387 Å and 106.17°, 105.15°, 92.60°] [41]. The close proximity of the values with each others may be due to the electronic delocalization effect resulted from the super-conjugation system formed in the whole TBI molecule.

The maximum difference for the bond lengths and angles between experimental reference and T1 is found to be 0.029 Å and 4.26°, respectively. The root mean square error (RMSE) is also found to be 0.015 Å for the bond lengths and 1.33° for angles. According to DFT calculations, the calculated geometric parameters of T1 were also compatible with the other corresponding compounds such as benzimidazole [42], 2-methyl-benzimidiazole [43] and thiophene [44]. These comparisons imply that the bond lengths and bond angles of the T1 tautomer are much closer to experimental data. Although the experimental results belong to solid phase, DFT-B3LYP results show a perfect fit with molecular structure parameters of the related compounds [40–44].

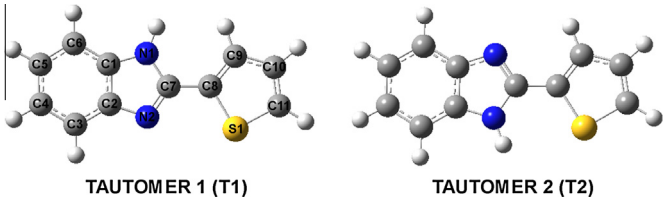

Fig. 1. The two stable tautomers of TBI molecule.

Table 1
The symmetry group, dipole moment in Debye, relative energies in kcal/mol and tautomeric mole fraction in percent of the possible stable tautomers of TBI.

Tautomers	B3LYP/6-311++G(d,p)[a]							
	Symmetry	μ_{total}	ΔE_{total}	ΔE_0	$\delta\Delta G$	$\delta\Delta G^*$	N_i	N_i^*
T1	C_s	3.606	–	–	–	–	28.00	28.34
T1	C_1	3.606	0.014	0.043	0.018	0.020	27.16	27.40
T2	C_s	2.823	0.441	0.445	0.029	0.051	26.66	26.01
T2	C_1	2.831	0.447	0.520	0.256	0.261	18.18	18.24

[a] The relative energies of the tautomers were given in respect to the total electronic energy (E_{total}), zero point corrected total energy (E_0), Gibbs free energy (ΔG) and thermal energy corrected Gibbs free energy (ΔG^*). For the T1 (C_s) tautomer, the E_{total}, E_0, ΔG and ΔG^* are −584744.017, −584640.932, −584664.737 and −584638.053 kcal/mol. N_i, is the tautomeric mole fraction.

Vibrational spectra

To the best of our knowledge, the vibrational wavenumbers and assignments for TBI have not been reported in the literature as yet. The infrared (ATR-IR and FT-IR), dispersive Raman spectra and the calculated vibrational spectra of T1 form in C_s point group symmetry are given in Figs. 2 and Fig. S2 (Supplementary material), respectively. The observed vibrational wavenumbers for TBI along with corresponding vibrational assignments and intensities are also given in Table 3; see also Table S1 (Supporting information) for a comprehensive description of all vibrational modes. All calculated wavenumber values presented in this study are obtained within the harmonic approximation, which allows us to describe vibrational motion in terms of independent vibrational modes that are governed by a simple one dimensional harmonic potential.

Table 2
Calculated skeletal bond lengths (Å) and bond angles (°) for the tautomers of TBI.

Parameter[a]	B3LYP/6-311++G(d,p)		
	T1 (C_s or C_1)	T2 (C_s or C_1)	Experimental [40]
Bond length			
C1—C2	1.415	1.415	1.395
C2—C3	1.399	1.393	1.392
C3—C4	1.389	1.391	1.383
C4—C5	1.408	1.408	1.392
C5—C6	1.392	1.389	1.381
C6—C1	1.393	1.400	1.387
C1—N1	1.383	1.382	1.394
C2—N2	1.382	1.383	1.393
C7—N1	1.384	1.315	1.376
C7—N2	1.315	1.384	1.316
C7—C8	1.448	1.450	1.457
C8—C9	1.377	1.374	1.362
C9—C10	1.421	1.420	1.392
C10—C11	1.368	1.367	1.345
C8—S1	1.744	1.750	1.728
C11—S1	1.729	1.732	1.707
Bond angle			
C1—C2—C3	119.77	122.58	119.58
C2—C3—C4	118.02	116.73	118.11
C3—C4—C5	121.44	121.48	121.42
C4—C5—C6	121.50	121.46	121.35
C5—C6—C1	116.75	118.03	116.83
C6—C1—N1	132.88	129.95	131.82
C2—C1—N1	104.60	110.34	105.84
C1—C2—N2	110.23	104.53	110.10
C3—C2—N2	130.00	132.89	130.32
C1—N1—C7	107.19	105.58	106.27
C2—N2—C7	105.67	107.23	105.10
N1—C7—C8	122.74	124.40	121.92
N2—C7—C8	124.94	123.28	124.98
C7—C8—C9	129.43	126.60	133.69
C7—C8—S1	119.65	122.79	116.83
C8—C9—C10	113.15	113.16	114.72
C8—S1—C11	91.30	91.61	91.81
C9—C10—C11	112.44	113.06	112.05
C10—C11—S1	112.19	111.56	112.13

[a] Coordinate descriptions are carried out by the numbers in Fig. 1.

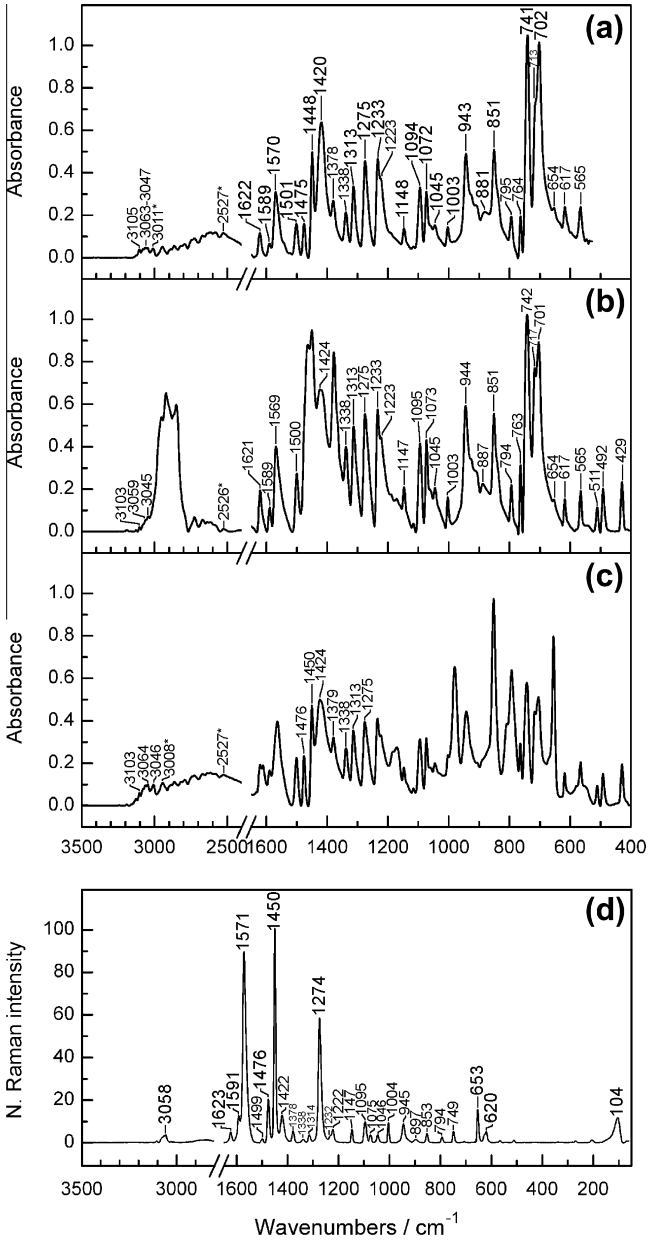

Fig. 2. The vibrational spectra of TBI: (a) ATR-IR spectrum; (b) FT-IR spectrum in Nujol mull; (c) FT-IR spectrum in hexachloro-1,3-butadiene mull; and (d) dispersive Raman spectrum.

Table 3
The observed vibrational wavenumbers (cm^{-1}) and assignments of TBI.

Mode, symmetry	Assignment[a]	Experimental[b]		
		IR(solid)	IR(Nujol)	Raman(solid)
59, A′	νC—H (r)	3105 vw	3103 vw[c]	
			3103 vw	
57, A′	νC—H (R)	3063 vw br	3064 w[c]	
			3059 vw sh	3058 vw
55, A′	νC—H (R)	3047 vw br	3046 w[c]	
			3045 vw	
52, A′	νC═C (R)	1622 w	1621 w	1623 vw
51, A′	νC═C (R)	1589 vw	1589 w	1591 w sh
50, A′	νC(R)—C(r)	1570 w	1569 m	1571 s
49, A′	νC═C (r)	1501 w	1500 w	1499 vw
48, A′	νC═C (R)	1475 w	1476 w[c]	1476 w
47, A′	νC═C (R)	1448 m	1450 m[c]	1450 vs
46, A′	νC═C (r)	1420 s	1424 m—s[c]	1422 w
45, A′	νC—N (R)	1378 w	1379 m[c]	1378 vw
44, A′	νC═C (R)	1338 w	1338 w—m[c]	1338 vw
42, A′	δC—H (R)	1313 m	1313 m[c]	1314 vw
41, A′	νC—N (R)	1275 m	1275 m	1274 m
40, A′	δC—H (r)	1233 m	1233 m	1232 vw sh
38, A′	δN—H	1223 m sh	1223 m sh	1222 vw
37, A′	δC—H (R)	1148 w	1147 w	1147 vw
36, A′	δC—H (R)	1094 m	1095 m	1095 vw
35, A′	δC—H (r)	1072 m	1073 m	1075 vw
34, A′	νC—N (R)	1045 w	1045 w	1046 vw
32, A′	νC═C (R)	1003 w	1003 w	1004 vw
30, A′	δCNC + δNCN (R)	943 m	944 m	945 vw
28, A′	δC—C—C (R)	881 w br	887 w br	897 vw br
26, A′	νC—S	851 m	851 m	853 vw
24, A″	γC—H (r)	795 w	794 w	794 vw
23, A′	νC═C (R)	764 w	763 m	
22, A″	γC—H (R)	741 vs	742 vs	749 vw
20, A″	γC—H (R)	713 s sh	717 s	
18, A″	γC—H (r)	702 vs	701 s	
17, A′	δ (r)	654 w sh	654 w sh	653 w
16, A′	δC—C—C (R)	617 w	617 w	620 vw
14, A″	γ (r)	565 w	565 w	
12, A′	δ (R)		511 w	
11, A″	τ (r)		492 w	
10, A″	τ (R)		429 w	

[a] R: benzimidazole ring, r: thiophene ring, ν: bond stretching, δ: in-plane angle bending, γ: out-of-plane angle bending, and τ: torsion.
[b] s: strong, m: medium, w: weak, v: very, sh: shoulder, and br: broad.
[c] The infrared active vibrational wavenumbers are obtained in hexachloro-1,3-butadiene.

TBI molecule consists of 22 atoms and has 60 fundamental vibrational modes belong to C_s point group; all of them are IR and Raman active [45]. These modes include 41 in-plane modes with A′ symmetry and 19 out-of-plane modes with A″ symmetry.

Due to various crystal interactions originated from solid phase recording, some of the vibrational bands are observed at different wavenumbers from the gas phase. Benzimidazole derivatives are known to be strongly associated through intermolecular hydrogen bonding. The ATR-IR spectrum of TBI shows strong bands in the 3010–2500 cm^{-1} region which indicate N—H···N type hydrogen bonds. These bands are characteristic for 1*H*-benzimidazole derivatives in the 3200–2400 cm^{-1} region [13,22,46]. In addition, the absence of any band for N—H stretching mode in the region of 3600–3200 cm^{-1} of the IR spectra of the compound indicates that o-phenylenediamine has reacted with the $NaHSO_3$ adduct of 2-thiophenecarboxaldehyde and formed the benzimidazole ring system. The free N—H stretching vibration is not observed in the region 3600–3400 cm^{-1}, but in-plane bending mode of N—H is assigned to the band observed at 1223 cm^{-1}.

The hetero aromatic structures show the presence of C—H stretching vibrations in the region 3100–3000 cm^{-1} which is the characteristic region for the ready identification of C—H stretching vibrations [46–48]. In this region, the bands are not affected appreciably by the nature of substituents [49]. The symmetric C—H stretching band of the thiophene ring is observed at 3105 cm^{-1} in the ATR-IR spectrum and 3103 cm^{-1} in Nujol or hexachloro-1,3-butadiene. The calculated value of this band was 3105 cm^{-1}. Two C—H stretching modes of benzimidazole ring are found at 3063 cm^{-1} and 3047 cm^{-1} in the ATR-IR spectrum. These bands were calculated at 3060 cm^{-1} and 3051 cm^{-1}. The counterpart of symmetric C—H stretching mode in the Raman spectrum is observed at 3058 cm^{-1}. The PED value ($\geqslant$97) of C—H stretching modes indicates that these are highly pure stretching modes.

The in-plane and out-of-plane C—H bending vibrations of the substituted benzene derivatives are expected in the wavenumber region 1300–1000 cm^{-1} and 1000–700 cm^{-1} [49]. The C—H in-plane bending vibrations of benzimidazole and thiophene rings were coupled with ring C—C and C═N stretching modes as evident from PED results. The C—H in-plane and out-of-plane bending vibrations were computed theoretically at 1293, 1222, 1134, 1101, 1076 cm^{-1} and 801, 755, 722, 689 cm^{-1}, respectively. IR active C—H in-plane bending vibrations of title molecule are observed at 1313, 1233, 1148, 1094 and 1072 cm^{-1}. The same vibrations in the Raman spectrum are assigned to the wavenum-

bers at 1314, 1232, 1147, 1095 and 1075 cm^{-1}. The corresponding C—H out-of-plane bending modes appear in the ATR-IR spectrum at 795, 741, 713, 702 cm^{-1} and in the Raman spectrum at 794 cm^{-1}. The experimental values are good agreement with theoretical values.

The aromatic carbon–carbon stretching vibration occurs in the region 1650–1200 cm^{-1} [49]. All substituted derivatives have bands in this region that vary in position and intensity with the nature and position of substituent. In the present work, the wavenumbers observed in the ATR-IR spectrum at 1622, 1589, 1501, 1475, 1448, 1420, 1338 cm^{-1} and in the Raman spectrum at 1623, 1591, 1499, 1476, 1450, 1422, 1338 cm^{-1} were assigned to aromatic C=C stretching vibrations. The computed wavenumber for C=C stretching vibrations were found in the range of 1608–1345 cm^{-1} (modes 52, 51, 49-46, 44).

The identifications of C=N and C—N stretching wavenumbers is a difficult task since there are problems in identifying these wavenumbers from other vibrations [26,49]. The calculations suggest that the expected C=N vibration may be probably mixing with aromatic C=C stretching modes of 52, 50, 48 and 46. However, the bands observed at 1378, 1275, 1045 cm^{-1} (IR) and at 1378, 1274, 1046 (Raman) cm^{-1} are assigned to C—N vibrations. These values support the reported results [14,22,23,40,46,50,51]

The C—S stretching vibration of the thiophene ring is observed at 851 cm^{-1} in the ATR-IR spectrum and 853 cm^{-1} in Raman spectrum in accordance with the literature [43,44,48,52]. The value of this band is calculated at 861 cm^{-1} with a PED of 41%.

The low wavenumber region generally gives more qualified information about the conformational behaviors of the compounds in any physical state [21,25,26]. Computational vibrational wavenumbers in this region (below 600 cm^{-1}) are sensitive than the high wavenumber region. As clearly seen from Table S1 (Supplementary material), the calculated wavenumbers are great agreement with the experimental ones. This agreement tends us to make more reliable vibrational assignment of title compound. The ring vibrations, such as in-plane, out-of-plane bending and torsion vibrations at 565, 511, 492 and 429 cm^{-1} are undoubtedly assigned.

To investigate the performance and vibrational wavenumbers for the title compound, the largest difference, RMSE and correlation (R) values between experimental and calculated vibrational wavenumbers were also calculated. For the unscaled wavenumbers, the largest difference, RMSE and R of the calculated bands were found to be 140 cm^{-1}, 48 cm^{-1} and 0.99954, whereas for the scaled wavenumbers by SQM were found to be 27 cm^{-1}, 13 cm^{-1} and 0.99962, respectively. It can be seen that the B3LYP calculation combined with SQM give more realistic results to interpret the vibrational wavenumbers of TBI molecule.

NMR Spectra

The ^{13}C, ^{1}H, DEPT-135 and HETCOR NMR spectra of TBI in DMSO-d_6 are shown in Fig. 3. The experimental ^{13}C and ^{1}H NMR chemical shifts (ppm) of TBI together within the calculated data for the tautomers in C_s and C_1 symmetry groups are given in Table 4. As can be clearly seen from that table, calculated data for all tautomers are nearly in accordance with the experimental values. This coherence shows that the molecule can be existed in each one of the tautomers without any symmetry restrictions in liquid phase.

As in Fig. 3a, TBI molecule shows eleven different carbon atoms, which is in agreement with the structure regarding the molecular symmetry. Due to that fact, in Fig. 3a, eleven carbon peaks are clearly observed between 147.00 and 111.11 ppm in ^{13}C NMR spectrum of TBI. The peaks at 147.00, 143.50, 134.67 and 133.59 ppm in ^{13}C NMR spectrum cannot be observed in DEPT 135 spectrum (Fig. 3b). Therefore, it can be concluded that these peaks belong to the four quaternary carbons of TBI. The signal at the lowest field (147.00 ppm) is assigned to C-7 carbon in C=N

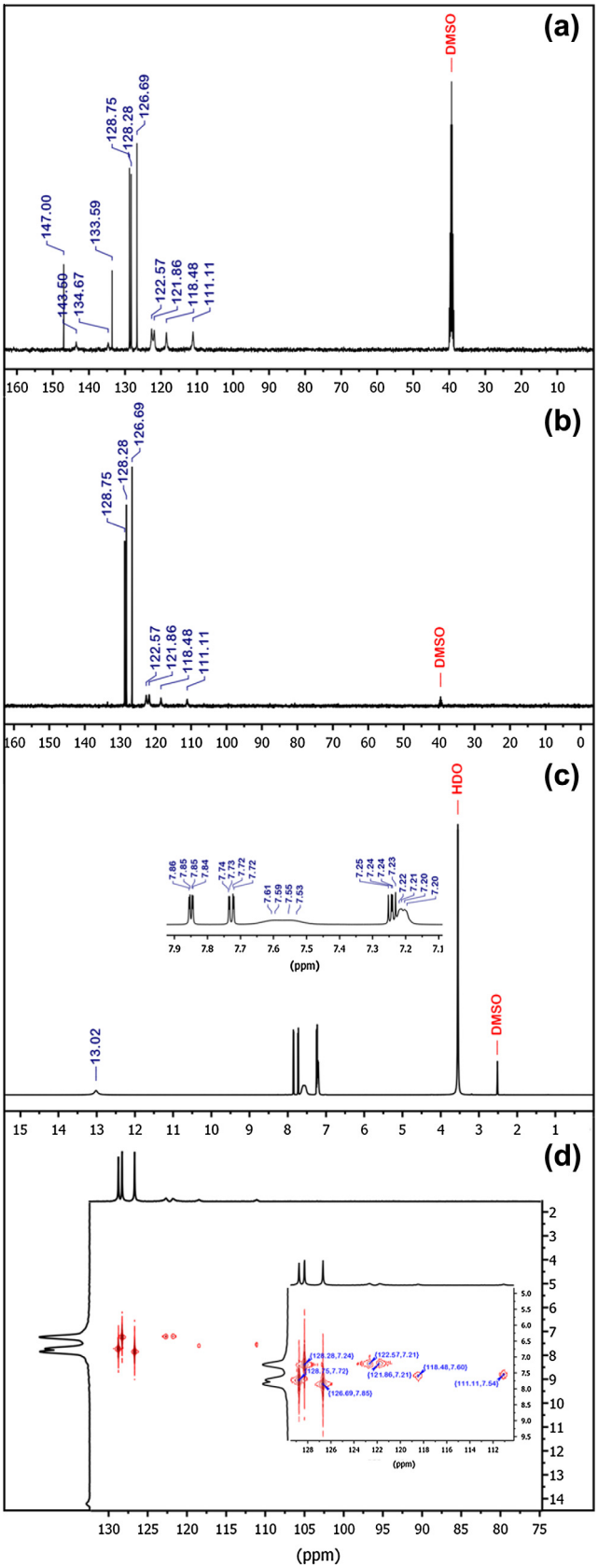

Fig. 3. The NMR spectra of TBI in DMSO-d_6: (a) ^{13}C; (b) DEPT-135; (c) ^{1}H; and (d) HETCOR.

Table 4
The experimental ^{13}C and ^{1}H NMR chemical shifts (ppm) together within the calculated data for the tautomers of TBI in DMSO-d_6.

Nucleus	Experimental	B3LYP/6-311++G(d,p)[a]			
		T1 (C_s)	T1 (C_1)	T2 (C_s)	T2 (C_1)
C-7	147.00	146.84	147.15	147.44	147.20
C-2	143.50	144.67	144.49	144.48	144.83
C-8	134.67	140.21	140.09	139.15	139.03
C-1	133.59	135.65	135.64	134.73	135.13
C11	128.75	135.50	135.45	134.28	134.07
C10	128.28	127.21	127.33	127.90	127.66
C9	126.69	126.03	125.10	129.06	127.78
C-5	122.57	123.57	124.07	123.84	124.07
C-4	121.86	122.67	123.01	123.23	123.56
C-3	118.48	118.83	119.05	118.62	118.91
C-6	111.11	110.73	110.85	110.51	110.86
H—N1	13.02	9.85	9.86	9.51	9.53
H—C9	7.85	7.84	7.77	8.33	8.25
H—C11	7.73	7.71	7.61	7.78	7.66
H—C3	7.60	7.80	7.78	7.75	7.80
H—C6	7.54	7.69	7.68	7.58	7.66
H—C10	7.24	7.27	7.27	7.36	7.32
H—C5	7.21	7.39	7.44	7.49	7.46
H—C4	7.21	7.39	7.46	7.47	7.47

[a] σ Transform into δ using equations given in Ref. [24] $\delta^{13}C = 175.7–0.963\ \sigma^{13}C$ and $\delta^{1}H = 30.9–0.970\ \sigma^{1}H$.

form which supports the formation of the benzimidazole ring. The other three signals of quaternary carbons at 143.50, 134.67 and 133.59 ppm are attributed to C-2, C-8 and C-1, respectively. All the other carbons in the compound appeared separately at the expected regions which support the structure of the TBI and in accordance with the reported values [22,23,26,40,43,53–55].

The protons of the benzimidazole ring appeared characteristically as broad signals, because of the presence of two tautomeric forms [53]. Broad appearance or merging of H—C3,6 and H—C4,5 together is also known to be the result of rapid proton exchange between N-1 and N-2 [53,55]. In Fig 3c, the broad peaks at 7.60 (bd), 7.54 (bd) and 7.21 (bdd) ppm are assigned to H—C3, H—C6 and H—C4/C5 in this manner. The correlations of thiophene ring are clearly observed in HETCOR spectrum (Fig. 3d). The cross peaks at 7.85, 7.73 and 7.24 ppm are easily assigned to thiophene ring protons as C-9, C-11 and C-10.

The experimental chemical shift (13.02 ppm) of proton attached to nitrogen shifted towards higher magnetic field by about 3.06–3.41 ppm, as compared with calculated value of tautomeric forms. This inconsistency should be due to the tautomerism, intermolecular or solute–solvent interactions. Therefore, it is difficult to predict accurately the theoretical NMR chemical shift of N—H proton.

Molecular electrostatic potential and natural population analysis

The molecular electrostatic potential (MEP) is related to the electronic density and is very useful descriptor for determining sites for electrophilic attack and nucleophilic reactions as well as hydrogen-bonding interactions [56,57]. To predict reactive sites for electrophilic and nucleophilic attack for the title molecule, MEP was calculated at the B3LYP/6-311++G(d,p) optimized geometry. The negative (red) regions of MEP were related to electrophilic reactivity and the positive (blue) regions to nucleophilic reactivity shown in Fig. S3 (Supplementary material). As can be seen from the figure, there is one possible site on the title compound for electrophilic attack. The negative region is localized on the unprotic nitrogen atom of the imidazole ring with a maximum value of −0.054 a.u. However, a maximum positive region is associated with protic nitrogen atom of the imidazole ring indicating a possible site for nucleophilic attack with a maximum value of 0.058 a.u. These results provide information concerning the region where the compound can interact with another molecule or a metal. So, Fig. S3 (Supplementary material) confirms the existence of an inter-molecular N—H···N interaction between the protic and unprotic N atoms of the imidazole ring in the solid state.

Additionally, main atomic charges (i.e. the charges on non hydrogen atoms computed by natural population analysis) were calculated at the same theory level and are listed in Table S2 (Supporting information). According to atomic charge results, the common atoms in both tautomers such as N1, N2, C11, C10, C6, and C8 possess richly negative charges, which are beneficial to the bioactivity [26].

Frontier molecular orbitals

Frontier molecular orbitals (FMOs), highest occupied molecular orbitals (HOMOs) and lowest unoccupied molecular orbitals (LUMOs), play an important role to characterize the chemical reactions [58]. FMOs are also used by the frontier electron density for predicting the most reactive position in π-electron systems and explain several types of reaction in conjugated systems. The HOMO energy characterizes the ability to donate an electron and LUMO energy characterizes the ability to obtain an electron. The energy gap between HOMO and LUMO is a critical parameter in determining the molecular chemical stability [58], optical properties [59] and biological activity [26].

The energies of the four important FMOs of tautomers: HOMO, HOMO−1, LUMO and LUMO+1 were calculated at B3LYP/6-311++G(d,p) theory level in order to understand the influence of the structural properties of TBI. The energy levels and distributions of the FMOs for each tautomer are presented Table S3 (Supporting information). The plots of the HOMOs and LUMOs are also depicted in Fig. S4 (Supplementary material). As can be seen from the figure, both the HOMO and LUMO are mainly delocalized among all the atoms. However, the HOMO−1 and LUMO+1 are partially localized on different parts of tautomers. The HOMO−1 orbitals are delocalized on the benzimidazole ring, while the LUMO+1 orbitals are delocalized on some atoms of the thiophene and imidazole rings. Both of the HOMOs and LUMOs are mostly π-antibonding-type orbitals. The energy gap value between HOMO and LUMO is found around 4.2 eV for the both tautomers. This value makes the TBI molecule chemically quite stable and reactive as antimicrobial.

Antimicrobial activity

The antimicrobial activity of the TBI compound was carried out using culture of *B. subtilis*, *S. aureus* as Gram positive bacteria and *E. coli*, *P. aeruginosa* as Gram negative bacteria and *S. cerevisiae* as yeast and *A. parasiticus*, *C. albicans* as fungus. The MIC determinations were obtained by broth microdilution assay. The results of antimicrobial activity of TBI are listed in Table S4 (Supporting information). MBC of TBI was equally effective against Gram-positive, Gram negative bacteria, fungus and yeast at the dose of >500 μg/ml. Due to the aggregation problem of the compound in some microorganisms, bacterial growth was not visible. For this reason, some microorganism's MIC values were not determined. However, the results clearly indicated that TBI compound has the capacity of inhibiting the metabolic growth of some bacteria investigated. TBI showed remarkable antibacterial activity against *P. aeruginosa* (MIC = 15.625 μg/ml) and antifungal activity against *A. parasiticus* (MIC = 125 μg/ml). It can be thought that the remarkable activity of this compound may be arising from the benzimidazole ring, which may play an important role in the antibacterial activity [13,60].

Conclusion

The conformational analysis results indicated that 2-(Thiophen-2-yl)-1*H*-benzo[*d*]imidazole has two stable tautomeric forms at room-temperature. According to the energy and stability analyses, Tautomer 1 (T1) in C_s symmetry is obtained as the more stable tautomeric form. The geometrical parameters and vibrational data of the T1 were also determined at DFT-B3LYP/6-311++G(d,p) theory level and were compared with experimental spectroscopic findings in the literature. The detailed interpretation of the vibrational spectra was carried out with the aid of scaled quantum mechanical method. The great match between experimental and calculated vibrational wavenumbers and intensities of each vibrational mode enables us to safely assign the fundamental bands. The infrared active continued band observed in the region 3010–2500 cm^{-1} is attributed to the N—H···N intermolecular hydrogen bonding interactions in solid state. To confirm the intermolecular interactions in liquid state, ^1H and ^{13}C chemical shifts of both tautomers in C_s and C_1 symmetry group were calculated at B3LYP/6-311++G(d,p) theory level and were compared with experimental values. The calculated NMR chemical shifts of both stable tautomers in C_s and C_1 symmetry groups were nearly consistence with the experimental values. This suggests that, the molecule could be existed in each one of two tautomers due to the intermolecular interactions or tautomerism in liquid phase. In addition, the broad appearance and/or merging together of some ^1H NMR shifts of the benzimidazole ring were obvious evidence for the rapid proton exchange between N-1 and N-2.

2-(Thiophen-2-yl)-1*H*-benzo[*d*]imidazole was also screened for its antimicrobial activity and found to be exhibit antifungal and antibacterial effects. The frontier molecular orbital, natural bond orbital and molecular electrostatic potential analyses were used to understand the activity of the title compound.

Acknowledgement

This study was supported financially by Bilecik Şeyh Edebali University (Project No: 2011-02-BİL.04-03).

Appendix A. Supplementary material

Supplementary data associated with this article can be found, in the online version, at http://dx.doi.org/10.1016/j.saa.2013.05.045.

References

[1] K.F. Ansari, C. Lal, Eur. J. Med. Chem. 44 (2009) 4028–4033.
[2] G. Ayhan-Kılcıgil, N. Altanlar, IL Farmaco 58 (2003) 1345–1350.
[3] S. Özden, D. Atabey, S. Yıldız, H. Göker, Bioorg. Med. Chem. 13 (2005) 1587–1597.
[4] M. Andrzejewska, L. Yepez-Mulia, R. Cedillo-Rivera, A. Tapia, L. Vilpo, J. Vilpo, Z. Kazimierczuk, Eur. J. Med. Chem. 37 (2002) 973–978.
[5] D.V. LaBarbera, E.B. Skibo, Bioorg. Med. Chem. 13 (2005) 387–395.
[6] H. Küçükbay, R. Durmaz, E. Orhan, S. Günal, IL Farmaco 58 (2003) 431–437.
[7] N.M. Agh-Atabay, B. Dulger, F. Gucin, Eur. J. Med. Chem. 38 (2003) 875–881.
[8] G. Navarrete-Vázquez, R. Cedillo, A. Hernández-Campos, L. Yépez, F. Hernández-Luis, J. Valdez, R. Morales, R. Cortés, M. Hernández, R. Castillo, Bioorg. Med. Chem. Lett. 11 (2001) 187–190.
[9] J. Cheng, J. Xie, X. Luo, Bioorg. Med. Chem. Lett. 15 (2005) 267–269.
[10] S.M. Sondhi, R. Rani, J. Singh, P. Roy, S.K. Agrawal, A.K. Saxena, Bioorg. Med. Chem. Lett. 20 (2010) 2306–2310.
[11] K.H. Hornberger, J.G. Badiang, J.M. Salovich, K.W. Kuntz, K.A. Emmitte, M. Cheung, Tetrahedron Lett. 49 (2008) 6348–6351.
[12] T.J. Lansing, R.T. McConnell, D.R. Duckett, G.M. Spehar, V.B. Knick, D.F. Hassler, N. Noro, M. Furuta, K.A. Emmitte, T.M. Gilmer Jr., R.A. Mook, M. Cheung, Mol. Cancer Ther. 6 (2007) 450–459.
[13] N.T. Abdel-Ghani, A.M. Mansour, Spectrochim. Acta A 86 (2012) 605–613.
[14] N. Sundaraganesan, S. Ilakiamani, P. Subramani, B. Dominic Joshua, Spectrochim. Acta Part A 67 (2007) 628–635.
[15] H. Arslan, Ö. Algül, Spectrochim. Acta A 70 (2008) 109–116.
[16] J.B. Foresman, A. Frisch, Exploring Chemistry with Electronic Structure Methods, second ed., Gaussian, Inc., Pittsburgh, 1996.
[17] W. Koch, M.C. Holthausen, A Chemist's Guide to Density Functional Theory, Wiley-VCH, 2000.
[18] A.D. Becke, J. Chem. Phys. 98 (1993) 5648–5652.
[19] H. Arslan, Ö. Algül, Y. Dündar, Vib. Spectrosc. 44 (2007) 248–255.
[20] R.K. Srivastava, V. Narayan, O. Prasad, L. Sinha, J. Chem. Pharm. Res. 4 (2012) 3287–3296.
[21] A. Ünal, M. Şenyel, Ş. Şentürk, Vib. Spectrosc. 50 (2009) 277–284.
[22] N. Özdemir, B. Eren, M. Dinçer, Y. Bekdemir, Mol. Phys. 108 (2010) 13–24.
[23] N. Özdemir, B. Eren, M. Dinçer, Y. Bekdemir, Int. J. Quantum Chem. 111 (2011) 3112–3124.
[24] H. Alyar, S. Alyar, A. Ünal, N. Özbek, E. Şahin, N. Karacan, J. Mol. Struct. 1028 (2012) 116–125.
[25] H. Alyar, A. Ünal, N. Özbek, S. Alyar, N. Karacan, Spectrochim. Acta Part A 91 (2012) 39–47.
[26] B. Eren, A. Ünal, Spectrochim. Acta Part A 103 (2013) 222–231.
[27] H.F. Ridley, R.G.W. Spickett, G.M.J. Timmis, Heterocycl. Chem. 2 (1965) 453–456.
[28] P. Gogoi, D. Konwar, Tetrahedron Lett. 47 (2006) 7982.
[29] National Committee for Clinical Laboratory Standards, Performance Standards for Antimicrobial Susceptibility Testing: Eleventh Informational Supplement, M100-S11, National Committee for Clinical Laboratory Standard, Wayne, PA, USA, 2003.
[30] S.A. Sarker, L. Nahar, Y. Kumarasamy, Methods 42 (2007) 321–324.
[31] C. Lee, W. Yang, R.G. Parr, Phys. Rev. B 37 (1988) 785–789.
[32] M.J. Frisch, et al., Gaussian 03 Revision D.01, Gaussian Inc., Wallingford, CT, 2004.
[33] D. Hur, A. Guven, J. Mol. Struct. – Theochem. 583 (2002) 1–18.
[34] SQM Version 1.0, Scaled Quantum Mechanical, 2013 Green Acres Road, Fayetteville, Arkansas 72703.
[35] J. Baker, A.A. Jarzecki, P. Pulay, J. Phys. Chem. A 102 (1998) 1412–1424.
[36] M. Cossi, V. Barone, B. Mennucci, J. Tomasi, Chem. Phys. Lett. 286 (1998) 253–260.
[37] J. Tomasi, B. Mennucci, E. Cances, J. Mol. Struct. – Theochem. 464 (1999) 211–226.
[38] K. Wolinski, J.F. Hinton, P. Pulay, J. Am. Chem. Soc. 112 (1990) 8251–8260.
[39] J.R. Cheeseman, G.W. Trucks, T.A. Keith, M.J. Frisch, J. Chem. Phys. 104 (1996) 5497–5509.
[40] D.K. Geiger, H.C. Geiger, L. Williams, B.C. Noll, Acta Cryst. E68 (2012) o420.
[41] M. Sekerci, Y. Atalay, F. Yakuphanoglu, D. Avcı, A. Basoglu, Spectrochim. Acta Part A 67 (2007) 503–508.
[42] M.A. Morsy, M.A. Al-Khaldi, A. Suwaiyan, J. Phys. Chem. A 106 (2002) 9196–9203.
[43] R. Infante-Castillo, L.A. Rivera-Montalvo, S.P. Hernandez-Rivera, J. Mol. Struct. 877 (2008) 10–19.
[44] K. Pasterny, R. Wrzalik, T. Kupka, G. Pasterna, J. Mol. Struct. 614 (2002) 297–304.
[45] F.A. Cotton, Chemical Applications of Group Theory, John Wiley & Sons, Inc., New York, 1965.
[46] P.N. Preston, The Chemistry of Heterocyclic Compounds: Benzimidazoles and Cogeneric Tricyclic Compounds, John Wiley & Sons. Inc., New York, 2009.
[47] G. Varsanyi, Assignments for Vibrational Spectra of Seven Hundred Benzene Derivatives, vol. 1, Adam Hilger, London, 1974.
[48] D. Lin-vien, N.B. Colthup, W.G. Fateley, J.G. Grasselli, The Hand Book of Infrared and Raman Characteristic Frequencies of Organic Molecules, Academic Press, New York, 1990.
[49] S. Sudha, M. Karabacak, M. Kurt, M. Cinar, N. Sundaraganesan, Spectrochim. Acta Part A 59 (2003) 2511–2517.
[50] C. James, C. Ravikumar, V.S. Jayakumar, I. Hubert Joe, J. Raman Spectrosc. 40 (2009) 537–545.
[51] T.D. Klots, P. Devlin, W.B. Collier, Spectrochim. Acta Part A 53 (1997) 2445–2456.
[52] V. Hernandez, F.J. Ramirez, J. Casado, F. Enriquez, J.J. Quirante, J.T. Lopez Navarrete, J. Mol. Struct. 410–411 (1997) 311–314.
[53] V. Sridharan, S. Saravanan, S. Muthusubramanian, S. Sivasubramanian, Magn. Reson. Chem. 43 (2005) 551–556.
[54] C.K. Lee, I.-S.H. Lee, Bull. Korean Chem. Soc. 29 (2008) 2205–2208.
[55] D.C.G.A. Pinto, C.M.M. Santos, A.M.S. Silva, Advanced NMR techniques for structural characterization of heterocyclic structures, in: M.V.D. Teresa (Ed.), Recent Research Developments in Heterocyclic Chemistry, Pinho e Melo, Research Signpost, Kerala (India), 2007.
[56] F.J. Luque, J.M. Lopez, M. Orozco, Theor. Chem. Acc. 103 (2000) 343–345.
[57] E. Scrocco, J. Tomasi, Adv. Quantum Chem. 11 (1978) 115–193.
[58] I. Fleming, Frontier Orbitals and Organic Chemical Reactions, Wiley, London, 1976.
[59] D. Sajan, K.U. Lakshmi, Y. Erdogdu, I.H. Joe, Spectrochim. Acta 78A (2011) 113.
[60] N.T. Abdel-Ghani, A.M. Mansour, Spectrochim. Acta A 81 (2011) 529–543.